

Alfvénic Velocity Spikes and Rotational Flows in the Near-Sun Solar Wind

J. C. Kasper^{1,2*}, S. D. Bale^{3,4,5}, J. W. Belcher⁶, M. Berthomier⁷, A. W. Case², B. D. G. Chandran^{8,9}, D. W. Curtis⁴, D. Gallagher¹⁰, S. P. Gary¹¹, L. Golub², J. S. Halekas¹², G. C. Ho¹³, T. S. Horbury⁵, Q. Hu¹⁴, J. Huang¹, K. G. Klein^{15,16}, K. E. Korreck², D. E. Larson⁴, R. Livi⁴, B. Maruca^{17,18}, B. Lavraud¹⁹, P. Louarn¹⁹, M. Maksimovic²⁰, M. Martinovic¹⁵, D. McGinnis¹², N. V. Pogorelov¹⁴, J. D. Richardson⁶, R. M. Skoug¹¹, J. T. Steinberg¹¹, M. L. Stevens², A. Szabo¹⁹, M. Velli²¹, P. L. Whittlesey⁴, K. H. Wright²⁵, G. P. Zank¹⁴, R. J. MacDowall¹⁹, D. J. McComas²², R. L. McNutt, Jr.¹³, M. Pulupa⁴, N. E. Raouafi¹³, and N. A. Schwadron^{8,9}

¹Climate and Space Sciences and Engineering, University of Michigan, Ann Arbor, MI 48109, USA

²Smithsonian Astrophysical Observatory, Cambridge, MA 02138, USA

³Physics Department, University of California, Berkeley, CA 94720-7300, USA

⁴Space Sciences Laboratory, University of California, Berkeley, CA 94720-7450, USA

⁵The Blackett Laboratory, Imperial College London, London, SW7 2AZ, UK

⁶Kavli Center for Astrophysics and Space Sciences, Massachusetts Institute of Technology, 77 Massachusetts Avenue Cambridge, MA 02139-4307, USA

⁷Laboratoire de Physique des Plasmas, CNRS, Sorbonne Université, Ecole Polytechnique, Observatoire de Paris, Université Paris-Saclay, Paris, 75005, France

⁸Department of Physics and Astronomy, University of New Hampshire, Durham, NH 03824, USA

⁹Space Science Center, University of New Hampshire, Durham, NH 03824, USA

¹⁰Heliophysics and Planetary Science Branch ST13, Marshall Space Flight Center, Huntsville, AL 35812, USA

¹¹Los Alamos National Laboratory P.O. Box 1663 Los Alamos, NM 87545, USA

¹²Department of Physics and Astronomy, University of Iowa, IA 52242, USA

¹³Johns Hopkins University Applied Physics Laboratory 11100 Johns Hopkins Road, Laurel, MD 20723-6099, USA

¹⁴Department of Space Science and Center for Space Plasma and Aeronomic Research, University of Alabama in Huntsville, Huntsville, AL 35805, USA

¹⁵Lunar and Planetary Laboratory, University of Arizona, Tucson, AZ 85721, USA

¹⁶Department of Planetary Sciences, University of Arizona, Tucson, AZ 85719, USA

¹⁷Department of Physics and Astronomy, University of Delaware, Newark, DE 19716, USA

¹⁸Bartol Research Institute, University of Delaware, Newark, DE 19716, USA

¹⁹NASA/Goddard Space Flight Center, Greenbelt, MD 20771, USA

²⁰LESIA, Observatoire de Paris, Université PSL, CNRS, Sorbonne Université, Université de Paris, 5 place Jules Janssen, 92195 Meudon, France

²¹Department of Earth, Planetary & Space Sciences, University of California, Los Angeles CA 90095, USA

²²Department of Astrophysical Sciences, Princeton University, Princeton, NJ 08544, USA

²⁴Institut de Recherche en Astrophysique et Planétologie, CNRS, UPS, CNES, Université de Toulouse, Toulouse, France

²⁵Universities Space Research Association, Science and Technology Institute, Huntsville AL 35805, USA

*jckasper@umich.edu

ABSTRACT

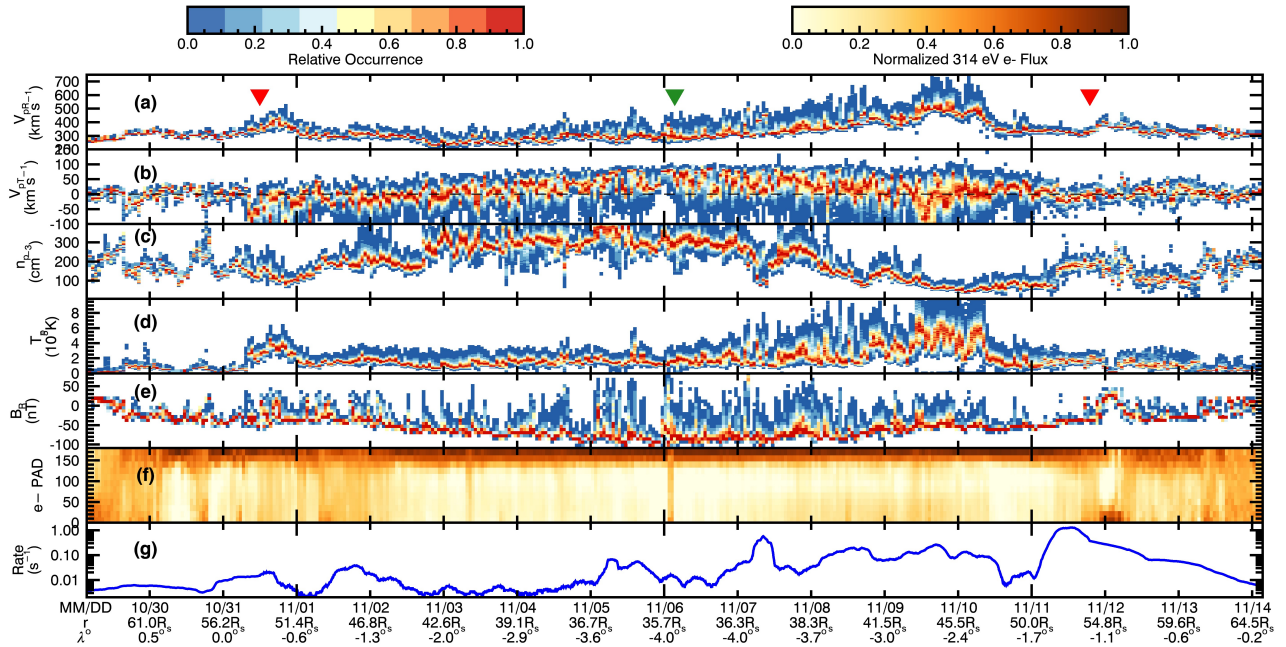


Figure 1. An overview of the first encounter with the Sun by Parker Solar Probe. (a) relative occurrence rate of proton radial speed V_{pR} in one hour intervals. Red triangles are the start and end of the high-rate data collection below $54R_S$ and the green triangle indicates perihelion at $35.7R_S$. (b) same for transverse component V_{pT} of proton velocity in solar equatorial plane, (c) proton number density n_p , (d) proton temperature T_p , (e) radial component of magnetic field B_R , (f) electron pitch-angle distribution, and (g) 20 – 200 keV proton rate. The date, distance r , and latitude λ relative to the solar equator are indicated at daily intervals.

The prediction of a supersonic solar wind¹ was first confirmed by spacecraft near Earth^{2,3} and later by spacecraft at heliocentric distances r as small as 62 solar radii (R_S)⁴. These missions showed that plasma accelerates as it emerges from the corona, aided by unidentified processes that transport energy outward from the Sun before depositing it in the wind. Alfvénic fluctuations are a promising candidate for such a process because they are seen in the corona and solar wind and contain significant energy^{5–7}. Magnetic tension forces the corona to co-rotate with the Sun, but to date any residual rotation reported far from the Sun has been much smaller than the amplitude of waves and deflections from interacting wind streams⁸. Here we report observations of solar-wind plasma at $r \simeq 35R_S$ ^{9–11}, well inside the radius at which stream interactions become important. We find that the Alfvén waves organize into structured velocity spikes up to minutes long that are associated with propagating S-like bends in the magnetic-field lines. We detect an increasing azimuthal flow velocity of the solar wind around the Sun, peaking at $35 - 50 \text{ km s}^{-1}$, significantly above the amplitude of waves. These flows exceed classical predictions of a few km s^{-1} , challenging models of circulation in the corona and calling into question our understanding of how stars lose angular momentum and spin down as they age^{12–14}.

Parker Solar Probe (PSP) launched in August 2018 on a Delta IV Heavy rocket. The high energy of the launch combined with a gravitational assist from Venus in September 2018, placed PSP into an eccentric orbit with a period of 147 days and a perihelion at $r = 35.7R_S$, nearly a factor of two closer to the Sun than any previous mission⁴. This letter makes use of observations collected by instruments on the spacecraft during the first two encounters with the Sun in November 2018 and April 2019. While the instruments collect observations at a low rate far from the Sun, the primary science collection at high rate occurs during the encounter phase of each orbit at $r < 54R_S$ (0.25 au). Encounter one (E1) lasted from 31 October to 12 November 2018, with the first perihelion occurring at 03:27 UT on 6 November. During these two encounters the longitude of PSP relative to the rotating surface of the Sun barely changed; PSP essentially dove down into, and then rose straight up from, a single narrow region above the Sun. E1 and E2 data thus describe a handful of specific solar-wind streams.

Nearly two million thermal energy distribution functions of the solar-wind protons were recorded during E1, and more than three times that during E2 (Fig. 1, Extended Data Figure 1). From these distribution functions solar wind proton bulk properties such as velocity, density, and temperature are derived. Within any hour interval, the distribution of radial solar-wind speed

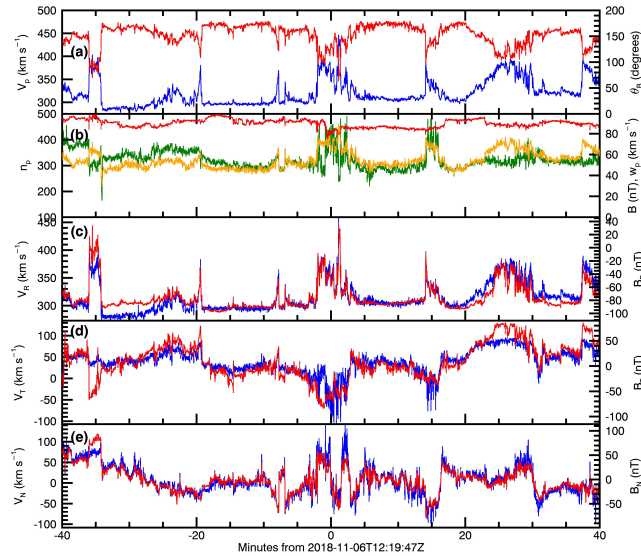


Figure 2. Solar wind fluctuations near closest approach. Near-Sun fluctuations meet Alfvénic criteria, but are organized into structures and contain density enhancements. (a) magnitude of V_{pR} (blue) and angle θ_{BR} of B from radial outwards, (b) magnitudes of n_p (green), B (red), and proton thermal speed w_p (yellow); (c-e) variation of each vector component of velocity (blue) and magnetic field (red) in the R , T , and N directions. There is a baseline solar wind speed with $\approx 300\text{km/s}$ and jets where V_p jumps by $\approx 100\text{km/s}$. The fluctuations are highly Alfvénic, with equal energy in field and flow, but organized into structures instead of randomly distributed, and there is evidence of compressions.

55 V_{pR} was strongly peaked at a minimum value, with a one-sided tail extending to larger V_{pR} . V_{pR} reached its minimum value of
56 200 km/s about a quarter of the way though E1 and then steadily rose to about 600 km/s. Numerical simulations and simple
57 extrapolations of the observed photospheric magnetic field suggest that PSP spent all of E1 south of the global heliospheric
58 current sheet (HCS), in a region with inward magnetic polarity ($B_R < 0$)¹⁵. Near the start and end of E1 PSP sampled slow
59 wind from near the HCS. Closer to the Sun PSP observed first very slow wind and then fast wind, both of which are thought
60 to emerge from a low-latitude coronal hole¹⁵. Below 40 R_S , V_{pT} has a net positive value, which peaks at closest approach.
61 This flow may be the long-sought signature of plasma co-rotation in the corona. The density peaks in the slowest wind, at
62 a value of approximately 400 cm^{-3} , about 50 times higher than typical values at 1 au, as expected from mass conservation
63 and spherical expansion. The proton temperature T_p and V_{pR} remain positively correlated¹⁶. At perihelion the protons are ≈ 4
64 times hotter than protons with similar V_{pR} at 1 au, consistent with radial scalings reported from earlier missions⁴. The radial
65 component of the magnetic field, B_R , increases in magnitude with proximity to the Sun but unexpectedly changes sign many
66 times. The pitch-angle (θ) distribution (PAD) for electrons, or the number of electrons at a given energy as a function of their
67 angle relative to B , is a valuable diagnostic of these changes in the direction of B . Here we show the PAD in a 22-eV-wide
68 energy channel centered on 314 eV, well above the electron thermal energy. The sharp peak near 180° corresponds to the *strahl*,
69 a beam of super-thermal electrons that travel away from the Sun along magnetic-field lines. Near the Sun *strahl* evolves towards
70 small $\sin \theta$ because of magnetic-moment conservation¹⁷. If the reversals in B_R seen by PSP result from PSP's crossing between
71 open field lines (connected to the Sun at only one end) with different signs of B_R back at the Sun, then the *strahl* would flip
72 between 180° and 0° each time B_R changed sign. Instead, every time B_R flips, the *strahl* maintains its 180° orientation, clearly
73 indicating that the reversals in B_R are due to S-like bends in the magnetic-field lines (Extended Data Figure 2). Closed field
74 lines with both ends connected to the Sun and *strahl* traveling both parallel and anti-parallel to B are seen during the arrival of a
75 coronal mass ejection on 12 November, following an enhancement in energetic particles¹⁸.

76 Fig. 2 shows a timeseries of 80 minutes of observations several hours after perihelion illustrating typical velocity and
77 magnetic-field fluctuations. About half the time B points radially inward towards the Sun and V sits at a relatively constant
78 300km/s . The remaining time includes seven distinct intervals in which B rotates away from its radial-inwards orientation

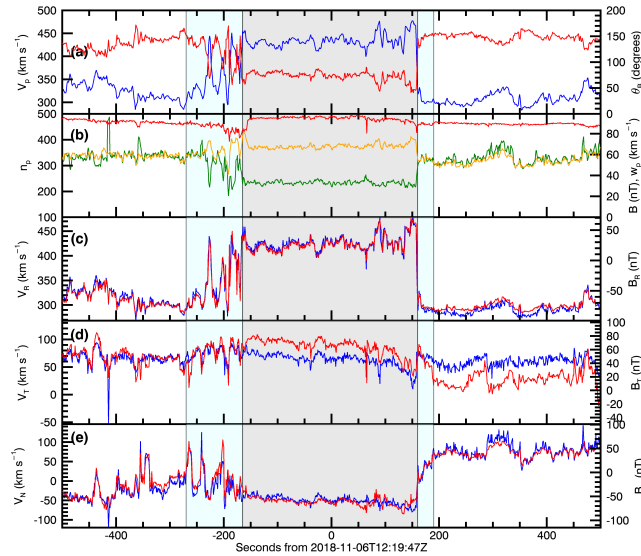


Figure 3. A closer look at a velocity spike. The same formatting is used as in Figure 2, but focused on a single 1,000 second interval. The left blue region indicates the 105 s period when PSP moved from the ambient plasma into the spike. The central core of the spike is indicated by the grey region and lasted for 325s, characterized by steady but disturbed flow and field with a large rotation in B to $\theta_B \sim 70^\circ$, a jump in flow to 343 km s^{-1} . Return from the core spike into ambient solar wind is marked by the second blue region and took 30s.

79 and V_{pR} simultaneously jumps and V also rotates, linking the one-sided tail in V_{pR} and the reversals in polarity seen in the E1
80 overview. These jumps in flow associated with rotations in B and V are similar to one-sided Alfvénic structures first seen farther
81 from the Sun^{6,7}. The spikes seen by PSP are different in that they have larger amplitudes and are often associated with an
82 increase in density, n_p , indicating that the spikes have a non-Alfvénic component. The correlated variations in the components
83 of B and V , their relative amplitudes, and the constant value of $|B|$ are consistent with large-amplitude, spherically polarized
84 Alfvén waves propagating through the plasma in the anti-Sunward direction, similar to earlier observations^{5,19}. We can classify
85 this wind stream (and indeed much of E1) as Alfvénic slow solar wind²⁰.

86 About 1,000 long-duration ($> 10 \text{ s}$) and isolated velocity spikes with large rotations in B were identified in E1. (About half
87 as many were seen in E2.) Often the spikes can be separated chronologically into a core region with plasma conditions that are
88 very different from the ambient solar wind but relatively constant, a comparatively short transition region on one side of the
89 core, and a longer transition region on the other side containing large-amplitude fluctuations (See Fig. 3). During the 105s
90 transition at the beginning of this spike the flow underwent seven large oscillations of amplitude 150 km s^{-1} , possibly resulting
91 from Kelvin-Helmholtz instability.

92 Equally unexpected as the spikes and B_R reversals are the large-amplitude and sustained positive rotational velocities seen
93 below $40R_S$ for E1 and $50R_S$ for E2 (Fig. 4). Net rotation has been reported farther from the Sun, but it was on the same order
94 as instrument error and much smaller than the standard deviation in flow due to fluctuations and stream interactions^{8,21}. Here
95 V_{pT} rises to 35 km s^{-1} (E1) and 50 km s^{-1} (E2). This is much greater than the variance from fluctuations including the velocity
96 spikes, there is no evidence of stream interactions, and the values are much greater than the precision in averaged flows of less
97 than 0.5 km s^{-1} and an absolute error in flow due to a pointing error of less than 3 km s^{-1} (See Methods). These are the first in
98 situ observations of net rotational flow in the solar wind significantly above fluctuations and uncertainty.

99 Some level of rotational flow has always been expected in the solar wind near the Sun, as magnetic tension in the corona
100 should force the plasma to rotate as the Sun spins. However, the large rotational velocities measured greatly exceed the value
101 in the axisymmetric Weber-Davis model¹³, posing a major challenge to our understanding of the dynamics of the near-Sun
102 solar wind. Determining the origin of these tangential flows will be essential for understanding how the Sun loses angular
103 momentum and spins down as it ages^{12,14,22}. Further studies of the angular momentum should include magnetic fields, waves,

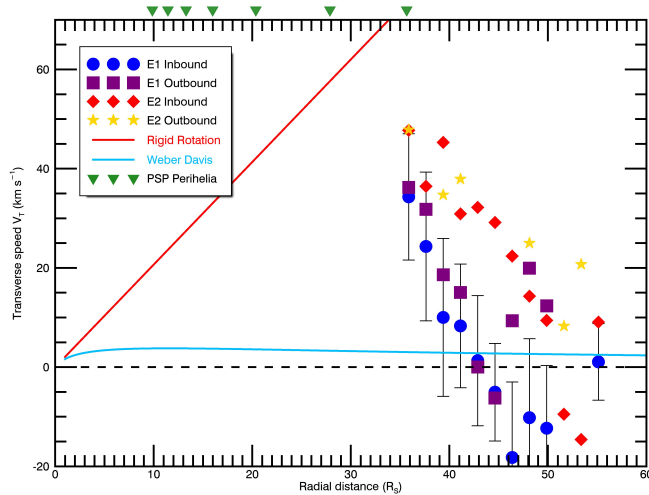


Figure 4. Large circulation of solar wind seen near Sun. Averaged rotational flow, V_{pT} , over $1.75R_{\odot}$ intervals during E1 (inbound in blue with error bars indicating standard deviation representative of all observations, outbound in purple) and E2 (inbound in red, outbound in yellow) as a function of radial distance. Each symbol is an average over at least 10,000 observations and the values closest to perihelion are averaged over 60,000–230,000 observations. Error bars for E1 inbound show one s.d. of the individual observations and are representative of the variation for the other 3 phases. The uncertainty in the mean of V_{pT} is much smaller than the symbols. Current and upcoming perihelia are shown with green triangles. Lines indicate no rotation (dashed), rigid co-rotation everywhere (red), and the axisymmetric Weber-Davis model (blue).

and other ions. Future PSP orbits will clarify the extent to which these large rotational flows characterize other solar-wind streams. These orbits will also provide critical additional diagnostics of the state of the plasma, including turbulence, velocity spikes, temperature anisotropy, and particle velocity-distribution functions, at heliocentric distances as small as $9.86R_{\odot}$.

References

1. Parker, E. N. Dynamics of the Interplanetary Gas and Magnetic Fields. *Astrophys. J.* **128**, 664–676 (1958).
2. Gringauz, K. I., Bezrokhikh, V. V., Ozerov, V. D. & Rybchinskii, R. E. A Study of the Interplanetary Ionized Gas, High-Energy Electrons and Corpuscular Radiation from the Sun by Means of the Three-Electrode Trap for Charged Particles on the Second Soviet Cosmic Rocket. *Soviet Physics Doklady* **5**, 361–364 (1960).
3. Bonetti, A., Bridge, H. S., Lazarus, A. J., Rossi, B. & Scherb, F. Explorer 10 Plasma Measurements. *J. Geophys. Res.* **68**, 4017–4063 (1963).
4. Marsch, E. *et al.* Solar wind protons - Three-dimensional velocity distributions and derived plasma parameters measured between 0.3 and 1 AU. *J. Geophys. Res.* **87**, 52–72 (1982).
5. Belcher, J. W. & Davis, J., Leverett. Large-amplitude Alfvén waves in the interplanetary medium, 2. *J. Geophys. Res.* **76**, 3534–3563 (1971).
6. Gosling, J. T., McComas, D. J., Roberts, D. A. & Skoug, R. M. A One-Sided Aspect of Alfvénic Fluctuations in the Solar Wind. *Astrophys. J. Lett.* **695**, L213–L216 (2009).
7. Horbury, T. S., Matteini, L. & Stansby, D. Short, large-amplitude speed enhancements in the near-Sun fast solar wind. *Mon. Not. Roy. Astron. Soc.* **478**, 1980–1986 (2018).
8. Pizzo, V. *et al.* Determination of the solar wind angular momentum flux from the HELIOS data - an observational test of the Weber and Davis theory. *apj* **271**, 335–354 (1983).
9. Fox, N. J. *et al.* The Solar Probe Plus Mission: Humanity’s First Visit to Our Star. *Space Sci. Rev.* **204**, 7–48 (2016).
10. Kasper, J. C. *et al.* Solar Wind Electrons Alphas and Protons (SWEAP) Investigation: Design of the Solar Wind and Coronal Plasma Instrument Suite for Solar Probe Plus. *Space Sci. Rev.* **204**, 131–186 (2016).
11. Bale, S. D. *et al.* The FIELDS Instrument Suite for Solar Probe Plus. Measuring the Coronal Plasma and Magnetic Field, Plasma Waves and Turbulence, and Radio Signatures of Solar Transients. *Space Sci. Rev.* **204**, 49–82 (2016).

- 129 **12.** Schatzman, E. A theory of the role of magnetic activity during star formation. *Annales d'Astrophysique* **25**, 18–29 (1962).
- 130 **13.** Weber, E. J. & Davis, J., Leverett. The Angular Momentum of the Solar Wind. *Astrophys. J.* **148**, 217–227 (1967).
- 131 **14.** Finley, A. J., Matt, S. P. & See, V. The Effect of Magnetic Variability on Stellar Angular Momentum Loss. I. The Solar
132 Wind Torque during Sunspot Cycles 23 and 24. *Astrophys. J.* **864**, 125 (2018).
- 133 **15.** Bale, S. D. *et al.* The magnetic structure and electrodynamics of the emerging solar wind. *Nature* (Submitted).
- 134 **16.** Elliott, H. A., Henney, C. J., McComas, D. J., Smith, C. W. & Vasquez, B. J. Temporal and radial variation of the solar
135 wind temperature-speed relationship. *Journal Geophysical Research: Space Physics* **117** A09102 (2012).
- 136 **17.** Pilipp, W. G. *et al.* Characteristics of electron velocity distribution functions in the solar wind derived from the helios
137 plasma experiment. *jgr* **92**, 1075–1092 (1987).
- 138 **18.** McComas, D. M. *et al.* Energetic Particle Environment near the Sun from Parker Solar Probe. *Nature* (Submitted).
- 139 **19.** Vasquez, B. J. & Hollweg, J. V. Formation of arc-shaped Alfvén waves and rotational discontinuities from oblique linearly
140 polarized wave trains. *J. Geophys. Res.* **101**, 13527–13540 (1996).
- 141 **20.** Bruno, R. & Carbone, V. The Solar Wind as a Turbulence Laboratory. *Living Reviews Solar Physics* **10**, 2 (2013).
- 142 **21.** Richardson, I. G. Solar wind stream interaction regions throughout the heliosphere. *Living Reviews Solar Physics* **15**, 1
143 (2018).
- 144 **22.** Axford, W. I. The Solar Wind. *Solar Physics* **100**, 575–586 (1985).

145 Figure Legends

146 **Figure 1:** An overview of the first encounter with the Sun by Parker Solar Probe.

147 (a) relative occurrence rate of proton radial speed V_{pR} in one hour intervals. Red triangles are the start and end of the
148 high-rate data collection below $54R_S$ and the green triangle indicates perihelion at $35.7R_S$. (b) same for transverse component
149 V_{pT} of proton velocity in solar equatorial plane, (c) proton number density n_p , (d) proton temperature T_p , (e) radial component
150 of magnetic field B_R , (f) electron pitch-angle distribution, and (g) 20 – 200 keV proton rate. The date, distance r , and latitude λ
151 relative to the solar equator are indicated at daily intervals.

152 **Figure 2:** Solar wind fluctuations near closest approach.

153 Near-Sun fluctuations meet Alfvénic criteria, but are organized into structures and contain density enhancements. (a)
154 magnitude of V_{pR} (blue) and angle θ_{BR} of B from radial outwards, (b) magnitudes of n_p (green), B (red), and proton thermal
155 speed w_p (yellow); (c-e) variation of each vector component of velocity (blue) and magnetic field (red) in the R , T , and N
156 directions. There is a baseline solar wind speed with $\approx 300\text{km/s}$ and jets where V_p jumps by $\approx 100\text{km/s}$. The fluctuations are
157 highly Alfvénic, with equal energy in field and flow, but organized into structures instead of randomly distributed, and there is
158 evidence of compressions.

159 **Figure 3:** A closer look at a velocity spike.

160 The same formatting is used as in Figure 2, but focused on a single 1,000 second interval. The left blue region indicates the
161 105 s period when PSP moved from the ambient plasma into the spike. The central core of the spike is indicated by the grey
162 region and lasted for 325s, characterized by steady but disturbed flow and field with a large rotation in B to $\theta_B \sim 70^\circ$, a jump in
163 flow to 343 km s^{-1} . Return from the core spike into ambient solar wind is marked by the second blue region and took 30s.

164 **Figure 4:** Large circulation of solar wind seen near Sun.

165 Averaged rotational flow, V_{pT} , over $1.75R_S$ intervals during E1 (inbound in blue with error bars indicating standard deviation
166 representative of all observations, outbound in purple) and E2 (inbound in red, outbound in yellow) as a function of radial
167 distance. Each symbol is an average over at least 10,000 observations and the values closest to perihelion are averaged over
168 60,000-230,000 observations. Error bars for E1 inbound show one s.d. of the individual observations and are representative
169 of the variation for the other 3 phases. The uncertainty in the mean of V_{pT} is much smaller than the symbols. Current and
170 upcoming perihelia are shown with green triangles. Lines indicate no rotation (dashed), rigid co-rotation everywhere (red), and
171 the axisymmetric Weber-Davis model (blue).

172 **Extended Data Figure 1:** An overview of the second encounter with the Sun by Parker Solar Probe.

173 In the same format as Fig. 1. Spikes in the velocity are again seen coincident with the magnetic field reversals, but the jump
174 in speed is smaller, likely because the Alfvén speed was slower in E2 than E1. The density at perihelion is substantially lower.

175 **Extended Data Figure 2:** Schematic of an "S-shaped" magnetic structure creating a field reversal, heat flux reversal, and
176 spike in velocity.

177 This figure illustrates the possible geometry of an "S-shaped" propagating Alfvénic disturbance (gray box) and how it
178 would appear to the spacecraft (black square) as it flew through the spike on the green trajectory. The light lines with arrows
179 indicate the configuration of the magnetic field, with all field lines ultimately pointed back to the Sun. Arrows at each black
180 square indicate the vector velocity (blue), electron strahl (orange), and magnetic field (red) seen by the spacecraft. If this was a
181 purely Alfvénic structure then the spike would move away from the Sun anti-parallel to B at the local Alfvén speed, C_A . In the
182 frame of the spike the shape of the structure would be static, with plasma flowing in along field lines on the upper left and
183 through the spike, emerging at the lower right, always flowing at C_A . In the frame of the spacecraft, the constant flow along
184 field lines in the propagating spike frame would translate into a radial increase of V by C_A when B was perpendicular to R , and
185 a maximum jump of $2C_A$ when B was completely inverted. Since the heat flux escapes away from the Sun, it would rotate so as
186 to always be anti-parallel to B and appear to be flowing back to the Sun at the center of this disturbance.

187 Methods

188 **Data Collection and Analysis** The data presented in this letter were collected over the course of the first two encounters of
189 the Sun by Parker Solar Probe in November 2018 and April 2019. This study makes use of all of the in situ instruments on
190 the spacecraft. Thermal plasma properties are measured by the PSP SWEAP instrument suite¹⁰, including the Solar Probe
191 (SPC) Cup, SPAN electron, and SPAN ion plasma data. Magnetic field data from the outboard FIELDS magnetometer was also
192 used^{11,15}, along with energetic particle rates as seen by $IS \odot IS$ ¹⁸. SPC measures the reduced distribution function of ionized
193 hydrogen and helium and the two dimensional flow angles of the ions as a function of energy/charge. These measurements are
194 performed at least once per second and typically more than four times per second throughout the encounter phase of each orbit
195 (below $0.25 au$ or $54 R_s$). This paper uses moments of the entire SPC proton distribution function to calculate a total effective
196 proton velocity, density, and radial component of the temperature. While the SPAN ion sensor generally did not view the peak
197 of the proton velocity distribution, the overlapping region seen by SPAN and SPC has been compared to confirm that there are
198 no gross offsets in calibration or derived plasma properties such as velocity, but this technique will be more accurate when the
199 solar wind flows into SPAN closer to the Sun. Observations of electrons with a center energy of 314 eV and width of 22 eV by
200 the two SPAN electron sensors were combined, along with the FIELDS determination of the magnetic field direction, to create
201 the electron pitch angle distributions.

202 All underlying data are being archived and will be available for download at the NASA Space Physics Data Facility in
203 November 2019²³. Additional SWEAP data and information are available at the SWEAP web page²⁴. Data were analyzed and
204 graphics developed in the Interactive Data Language (IDL).

205 **Statistics** The distributions of plasma properties in Fig. 1 and Extended Data Figure 1 were produced with one hour
206 time resolution. During the encounters the time resolution of the plasma instrument ranged from slightly more than one
207 measurement per second to more than four measurements per second, so each column in those panels represents the distribution
208 of approximately 3,600-14,400 measurements. All error bars indicate one standard deviation (s.d.) of the measurements from
209 the mean. At least 10,000 and generally more than 80,000 observations are used in calculating the mean transverse flow V_{pT} in
210 Figure 4.

211 **Estimates of Uncertainty** The absolute accuracy of the Solar Probe Cup (SPC) ion measurements are summarized here.
212 As verified in ground testing, the absolute accuracy for V_{pR} is less than 0.01% over a measurable range of approximately 119
213 km/s to 1065 km/s. The absolute accuracy in temperature is similarly negligible over a measurable range of approximately
214 7.3 kK to 21.1 MK (i.e. thermal speeds of 11 km/s to 600 km/s). Speeds and temperatures at the extremes of these ranges
215 are subject to systematic considerations, but no such measurements have been presented here. The accuracy of the density
216 measurement is determined by comparison with the plasma frequency as observed by FIELDS¹¹. Thus the absolute accuracy
217 of the SPC density measurement is estimated at $\approx 1\%$ and is no worse than 3%. The absolute accuracy for off-radial flow
218 components are verified via spacecraft roll maneuvers about the SPC symmetry axis. For solar wind fluxes typical of the first
219 two encounters, the uncertainty associated with this calibration corresponds to a typical absolute accuracy of ≈ 0.5 degrees.
220 For $400 km s^{-1}$ solar wind this corresponds to an expected error in V_{pT} of $3 - 4 km s^{-1}$, which is much smaller than the net
221 rotational flow observed.

222 **Signatures of Alfvénic Fluctuations** In discussing Fig. 2 we stated that the correlation of fluctuations in components
223 of \mathbf{B} and \mathbf{V} were generally indicative of outward propagating Alfvén waves. Consider vector waves or fluctuations $\Delta\mathbf{V}$ and
224 $\Delta\mathbf{B}$ superimposed on a steady background \mathbf{B}_0 and \mathbf{V}_0 . In the long wavelength fluid magnetohydrodynamic (MHD) limit
225 Alfvén waves propagate exactly parallel or anti-parallel to \mathbf{B}_0 , are dispersionless and do not compress the plasma, and there
226 is a simple linear relationship $\Delta\mathbf{B} = \pm D_A \Delta\mathbf{V}$, where $D_A = (n_p + 4n_\alpha)^{0.5} \Theta / 21.8 (nT km^{-1} s)$, densities are in units of cm^{-3} ,
227 and $\Theta = (1 - \beta_{\parallel} + \beta_{\perp})^{-0.5}$. Here Θ is a correction for thermal pressure anisotropy where β_{\parallel} is the ratio of parallel plasma
228 pressure to magnetic pressure and β_{\perp} is the ratio of perpendicular plasma pressure to \mathbf{B} . For this period we find that on average

229 $n_p = 220 \text{ cm}^{-3}$, $\beta_{\parallel} = 0.202$, and $\beta_{\perp} = 0.315$. SPC and SPAN were not configured optimally to measure the ionized helium
230 abundance n_{α} , so assuming the typical range $0.5 < n_{\alpha}/n_p < 4.5\%$ we expect $D_A = 0.68 - 0.74 \text{ (nT km}^{-1} \text{ s)}$. We find D_A for
231 each of the *RTN* components to be 0.71, 1.09, 0.70 $\text{(nT km}^{-1} \text{ s)}$, so the *R* and *N* components are exactly within the expected
232 range and the fluctuations in the *T* direction are about 33% higher. It is common for the D_A to be different for each component
233 of the velocity⁵. We then used the calculated value of D_A to rescale the range of the vector components of *B* so they should
234 overlap with *V* if the fluctuations were purely Alfvénic. The sign of the relation between ΔB and ΔV is given by the sign of
235 $-\mathbf{k} \cdot \mathbf{B}_{\odot}$, where *k* is the wavevector and gives the direction of propagation, and *B* is an average direction of the field over a long
236 time scale. Since the ambient direction of the magnetic field outside the large amplitude fluctuations points towards the Sun and
237 the correlations are overwhelmingly positive this means we are seeing outward waves.

238 **Identification of velocity spikes.** Isolated velocity spikes were identified by looking for all intervals in each encounter
239 where the orientation of the magnetic field started in the quiet configuration pointed nearly towards the Sun, rotated more than
240 45° away from the quiet configuration for at least 10 seconds, and then returned back to the original direction. Candidate events
241 were then examined manually to identify starting and ending times.

242 Methods References

243 23. NASA's Space Physics Data Facility <https://spdf.gsfc.nasa.gov/>.

244
245 24. The SWEAP Suite on Parker Solar Probe <https://www.cfa.harvard.edu/sweap>.

246 Acknowledgements

247 The SWEAP Investigation and this publication are supported by the PSP mission under NASA contract NNN06AA01C. The
248 SWEAP team expresses its gratitude to the scientists, engineers, and administrators who have made this project a success,
249 both within the SWEAP institutions and from NASA and the project team at JHU/APL. J.C.K. acknowledges support of the
250 2019 Summer School at the Center for Computational Astrophysics, Flatiron Institute. The Flatiron Institute is supported by
251 the Simons Foundation. S.D.B. acknowledges the support of the Leverhulme Trust Visiting Professorship program. TH was
252 supported by UK STFC ST/S0003641/1.

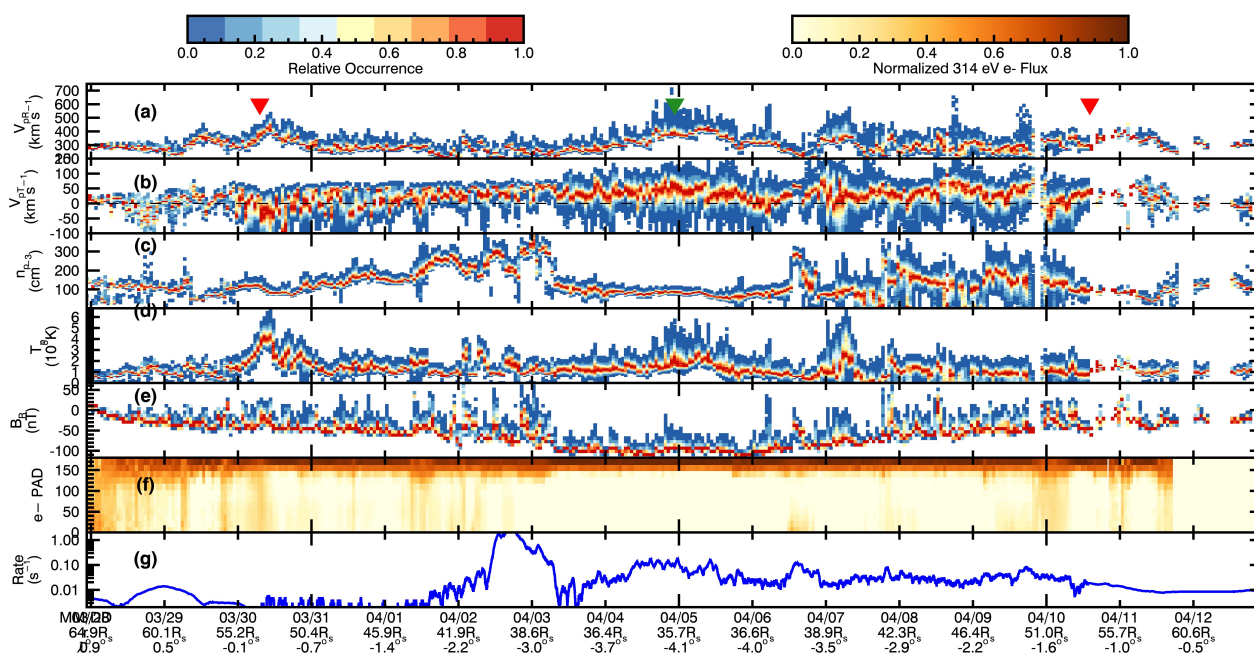
253 Author contributions statement

254 J.C.K. is the SWEAP Principal Investigator and led the data analysis and writing of this letter. S.D.B. is the FIELDS PI and a
255 SWEAP Co-Investigator and provided the magnetic field observations. J.W.B. leads the US group where the solar wind Faraday
256 cup was developed and provided guidance on identifying Alfvénic fluctuations. M.B. provided a pre-amplifier ASIC used
257 within the SPAN electron instruments. A.W.C. is the Solar Probe Cup instrument scientist and ensured that the instrument met
258 its performance requirements and was calibrated. B.D.G.C. contributed theoretical calculations and writing to the manuscript.
259 D.W.C. D.G. was the institutional lead at NASA MSFC responsible for materials testing and calibration of SPC. S.P.G. provided
260 recommendations on measurement requirements in order to detect instabilities. L.G. provided related solar observations and
261 results. J. H. contributed to the analysis of the electron observations and to the manuscript. G.H. provided a time of flight
262 ASIC to reduce the size and power of the SPAN ion instrument. T.H. participated in the analysis of the Alfvénic spikes.
263 Q.H. identified magnetic flux ropes. K.G.K. contributed to writing the manuscript and provided warm plasma growth rate
264 calculations. K.E.K. led the SWEAP Science Operations Center and coordinated observing plans between the instruments
265 and the project. M.V. contributed to writing the manuscript and discussing the relationship between Alfvénic fluctuations and
266 angular momentum. D.L. is the institutional lead at Berkeley responsible for the implementation of the SPAN instruments and
267 the SWEAP Electronics Module suite-wide computer. R.L. is the SPAN ion instrument scientist. B.A.M. performed simulations
268 of the fields of view of the SWEAP ion instruments and their probabilities of detecting the solar wind. B.L. identified flux
269 ropes and other signatures of coronal mass ejections in the data. P.L. coordinated solar furnace testing of the Solar Probe Cup
270 materials before launch. M.M. absolute calibration, quality of vdfs. N.P. Numerical simulations. J.D.R. FC design, radial
271 variation. R.K.S. Electron PADs. J.T.S. field rotation causes. M.L.S. Overall data pipeline for SWEAP, SPC high level data
272 products. A.S. estimated the location of the heliospheric current sheet. P.W. set up the SPC calibration at MSFC and then
273 became SPAN electron instrument scientist at Berkeley. K.W. arranged the SPC calibration at MSFC. G.P.Z. leads the SWEAP
274 theory team. R.J.M. leads the FIELDS fluxgate magnetometer. D.J.M. is the IS \odot IS PI. He provided the energetic particle data.
275 R.M. Lead for the EPI-Lo energetic particle instrument. M.P. FIELDS SOC lead. N.R. PSP Project Scientist and reviewed
276 jets and similar coronal transients. N.A.S. runs the IS \odot IS Science Operations Center. All authors participated in planning
277 the observations and data collection, reviewed and discussed the observations, and read, provided feedback, and accepted the
278 contents of the manuscript.

279 **Author Information**

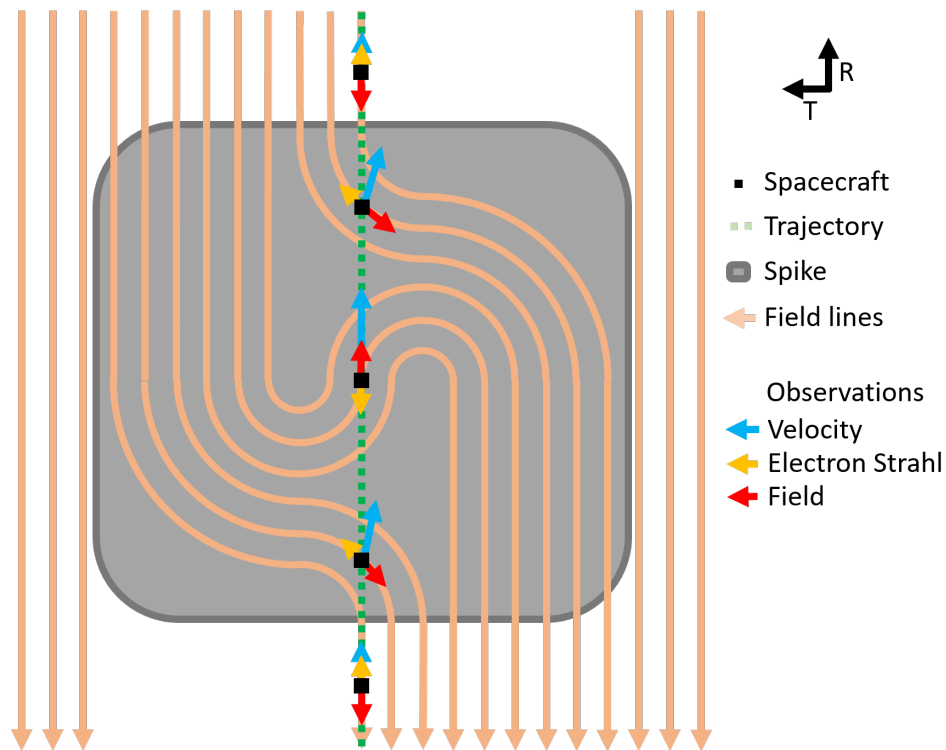
280 Correspondence and requests for materials should be addressed to Justin Kasper (jckasper@umich.edu). Reprints and
 281 permissions information is available at www.nature.com/reprints. The authors declare no competing financial interests. Readers
 282 are welcome to comment on the online version of the paper. Publisher’s note: Springer Nature remains neutral with regard to
 283 jurisdictional claims in published maps and institutional affiliations. None of the authors has a competing financial interest in
 284 this work.

285 **Extended Data – Online Supporting Materials**



287 **Extended Data Figure 1:** An overview of the second encounter with the Sun by Parker Solar Probe.
 288

288 In the same format as Fig. 1. Spikes in the velocity are again seen coincident with the magnetic field reversals. A net
 289 positive V_{PT} is seen at the second perihelion.



290
291
292
293
294
295
296
297
298
299
300
301
302

Extended Data Figure 2: Schematic of an “S-shaped” magnetic structure creating a field reversal, heat flux reversal, and spike in velocity.

This figure illustrates the possible geometry of an “S-shaped” propagating Alfvénic disturbance (gray box) and how it would appear to the spacecraft (black square) as it flew through the spike on the green trajectory. The light lines with arrows indicate the configuration of the magnetic field, with all field lines ultimately pointed back to the Sun. Arrows at each black square indicate the vector velocity (blue), electron strahl (orange), and magnetic field (red) seen by the spacecraft. If this was a purely Alfvénic structure then the spike would move away from the Sun anti-parallel to B at the local Alfvén speed, C_A . In the frame of the spike the shape of the structure would be static, with plasma flowing in along field lines on the upper left and through the spike, emerging at the lower right, always flowing at C_A . In the frame of the spacecraft, the constant flow along field lines in the propagating spike frame would translate into a radial increase of V by C_A when B was perpendicular to R , and a maximum jump of $2C_A$ when B was completely inverted. Since the heat flux flows away from the Sun, it would rotate so as to always be anti-parallel to B and appear to be flowing back to the Sun at the center of this disturbance.